Decentralized Coordination and Stabilization of Hybrid Energy Storage Systems in DC Microgrids

Mengfan Zhang, *Member, IEEE*, Qianwen Xu, *Member, IEEE*, Chuanlin Zhang, *Senior Member, IEEE*, Lars Nordström, *Senior Member, IEEE*, and Frede Blaabjerg, *Fellow, IEEE*

***Abstract*—Hybrid energy storage system (HESS) is an attractive solution to compensate power balance issues caused by intermittent renewable generations and pulsed power load in DC microgrids. The purpose of HESS is to ensure optimal usage of heterogeneous storage systems with different characteristics. In this context, power allocation for different energy storage units is a major concern. At the same time, the wide integration of power electronic converters in DC microgrids would possibly cause the constant power load instability issue. This paper proposes a composite model predictive control based decentralized dynamic power sharing strategy for HESS. First, a composite model predictive controller (MPC) is proposed for a system with a single ESS and constant power loads (CPLs). It consists of a baseline MPC for optimized transient performance and a sliding mode observer to estimate system disturbances. Then, a coordinated scheme is developed for HESS by using the proposed composite MPC with a virtual resistance droop controller for the battery system and with a virtual capacitance droop controller for the supercapacitor (SC) system. With the proposed scheme, the battery only supplies smooth power at steady state, while the SC compensates all the fast fluctuations. The proposed scheme achieves a decentralized dynamic power sharing and optimized transient performance under large variation of sources and loads. The proposed approach is verified by simulations and experiments.**

***Index Terms*—Hybrid energy storage system, pulsed power load, constant power load, stability, decentralized control, model predictive control.**

I. Introduction

MICROGRIDS, serve as the fundamental blocks for the future smart grids, provide an efficient integration of renewable energy resources (RESs), electric loads and energy storage systems (ESSs) [1]. As most RESs and ESSs are DC by nature and there are increasing penetration of DC loads (e.g., LED lighting, motor drive systems, data center), DC microgrids have gained a lot of attention nowadays [2]. Due to their advantages in flexibility, high efficiency, high controllability and high power density delivery capability, DC microgrids have wide applications in residential/commertial buildings, and onboard power systems like more electric aircraft, electric vehicles and all electric ships [3].

In DC microgrids, it is important to maintain supply demand balance with the intermittent outputs of RESs and the rapid/uncertain variation of loads (e.g., pulsed power loads) [4]. ESSs are commonly applied to address the power imbalance issue. Different ESSs have different charcteristics, e.g., batteries have high energy density but slow dynamic response and low power density; supercapacitors (SCs) have high power density, fast dynamics but low energy density. Hybridization of different ESSs with complementary characteristics provides a promising solution [5]. For example, hybrid battery/SC systems are widely applied in DC microgrids to compensate renewable fluctuations and pulsed power loads with high energy density, high power density and fast dynamics at the same time.

To maximize the utlization of hybrid energy storage systems (HESSs), a major challenge is the power allocation of different ESSs. Based on their characteristics, it is expected that the battery only supplies smooth power, while the SCs compensate all the fast fluctuations in the system. Many strategies have been reported in previous literature, including filter-based approaches [6], model predictive control [7], wavelet transformation [8], optimization based methods [9], [10]. However, all these methods require a central controller to generate current references for local converter controllers of individual ESS systems through communication networks, and the local controllers track the current references based on local converter control. They encounter the issues of communication delay/failures as well as low scalability. To enhance scalability, reliability and economy, decentralized control methods are proposed as alternatives to centralized control. Extended droop control schemes are proposed for hybrid battery/SC systems in [11]–[13], which utilize the characteristics of droop control and extended droop control (virtual resistance/capacitance droop) to achieve decentralized dynamic power sharing. However, for all these methods, either centralized or decentralized, the local controllers of ESS converters are controlled by PI controllers, which are designed based on

Manuscript received July 18, 2021; revised October 28, 2021; accepted November 28, 2021. Date of publication January 14, 2022; date of current version April 22, 2022. This work was supported in part by the StandUP for Energy, Sweden and in part by the Shanghai Rising-Star program under Grant 20QA1404000. Paper no. TSG-01135-2021. *(Corresponding author: Chuanlin Zhang.)*

Mengfan Zhang, Qianwen Xu, and Lars Nordström are with the Electric Power and Energy Systems Division, KTH Royal Institute of Technology, 114 28 Stockholm, Sweden (e-mail: mezhang@kth.se; qianwenx@kth.se; larsno@kth.se).

Chuanlin Zhang is with the Intelligent Autonomous Systems Lab, Shanghai University of Electric Power, Shanghai 201399, China (e-mail: clzhang@shiep.edu.cn).

Frede Blaabjerg is with the Department of Energy Technology, Aalborg University, 9220 Aalborg, Denmark (e-mail: fbl@et.aau.dk).

Color versions of one or more figures in this article are available at https://doi.org/10.1109/TSG.2022.3143111.

Digital Object Identifier 10.1109/TSG.2022.3143111

small signal models around a certain operating point. They cannot guarantee system performance with large disturbances of the operating point.

There is another challenge related to the stability issue caused by the wide utilization of power electronic converters to interface ESSs and loads [14]. The tightly controlled power electronic converter loads behave as CPLs (e.g., inverter fed motor drive systems, and converter fed loads), which has negative impedance feature and might destabilise the system [15]. To address this issue, many works have been conducted. The research in [16] shows that passive damping approaches can effectively increase system damping by adding passive elements (e.g., resistors, capacitors or proper LC filters). However, these methods would cause additional weight, losses and costs, while the damping are usually limited by physical constraints. The utilization of electric springs also provide an alternative solution by stabilizing grids through active control of loads [17]–[19]. But they require additional hardware circuits and the tradeoff is the unsatisfaction of load demand. Active damping methods can stabilize the system by adding equivalent virtual impedance dampings through modifying the proper control loops [20]. However, these approaches are depend on the linearized small signal models, thus they can only ensure small signal stability at the fixed operating point. To stabilize the system in a large signal sense considering the nonlinearty of power electronic converters and CPLs, several nonlinear approaches have been proposed, such as sliding mode control [21], composite backstepping control [22], [23], adaptive passivity based control [24], etc. However, for all above mentioned nonlinear control methods, the design of control parameters rely on empirical experience, and they cannot guarantee the optimal performance with smooth transients (e.g., small settling time and small overshoot). In a previous work [25], a MPC based controller is developed as a preliminary work to address this issue with some simulation results, but it requires further analysis and experimental results for verification. A MPC controller is developed in [26] for a buck converter with experimental verification, but this method is not scalable for other types of DC/DC converters. Moreover, all these approaches are only suitable for single DC/DC converter systems with one energy source, without considering system level coordination for multiple energy sources. For the HESS with more than one energy sources, it is clearly of significance to develop a system level control scheme with optimized control performance as well as large signal stability.

This paper proposes a composite MPC based coordination strategy to achieve decentralized dynamic power sharing of HESS, taking into consideration the stability issue caused by CPLs. First, a composite MPC controller is proposed to stabilize a single ESS system. It consists of a baseline MPC for fast and smooth transient performance and a higher-order sliding mode observer for large signal disturbance rejection. Next, the composite MPC controller is integrated with a virtual capacitance/resistance droop controller to achieve dynamic power sharing between battery and SC to make sure that the battery only provides the smooth power at the steady state while the SC compensates for all the fast fluctuations. The proposed control scheme achieves decentralized dynamic power sharing with fast dynamics, optimized transient performance and guaranteed stability under large disturbances.

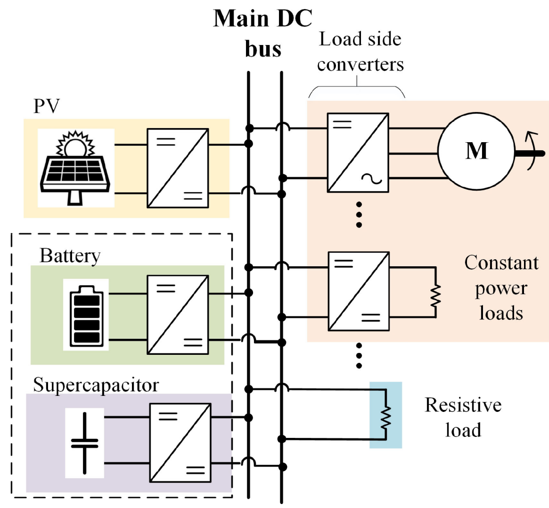

Fig. 1. A typical DC microgrid with the integration of a hybrid energy storage system.

This paper is organized as follows: The system model and problem description are shown in Section II. A composite MPC controller is proposed for a single ESS system in Section III. A composite MPC based decentralized dynamic power sharing strategy for HESS is developed in Section IV. Simulation and experimental verifications are shown in Section V and VI, respectively. Conclusions are drawn in Section VII.

II. System Model and Problem Description

Fig. 1 shows a typical DC microgrid with the integration of HESS. A battery and a SC are connected to the DC bus through respective bidirectional DC/DC converters. The PV is represented by a lumped constant power source (CPS), which operates at maximum power point tracking mode. There are various power converter loads, including inverter fed motor drive system and DC/DC converter fed resistive loads. These tightly controlled converter loads are typical CPLs with destabilizing effects. The CPLs and CPS can be represented as a lumped CPL, which is denoted as P_{CPL} (P_{CPL} can be either positive or negative; when it is negative, it means renewable generation is larger than consumption of constant power loads). The resistive loads are lumped as a resistor R. The HESS will support DC bus and compensate imbalanced power between PV and loads. Thus the currents at DC bus is written as

$$\begin{cases} i_{oB} + i_{oSC} = i_o \\ i_o = \frac{P_{CPL}}{v_{dc}} + \frac{v_{dc}}{R} \end{cases} \quad (1)$$

where i_{oB} and i_{oSC} represent the output currents of battery converter and SC converter, respectively; i_o is the equivalent load current of HESS, i_o can be either positive or negative; v_{dc} represents the DC bus voltage.

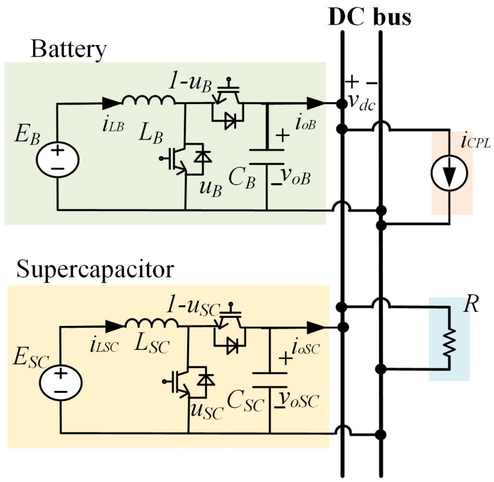

Fig. 2. A simplified DC microgrid with a hybrid energy storage system.

The system in Fig. 1 can be simplified as shown in Fig. 2. Then the HESS system model can be expressed as

$$\begin{aligned} L_i\frac{di_{Li}}{dt} &= E_i - (1-u_i)v_{Ci} \\ C_i\frac{dv_{Ci}}{dt} &= (1-u_i)i_{Li} - i_{oi} \end{aligned} \tag{2}$$

where E_i, v_{Ci}, i_{Li}, i_{oi}, L_i, and C_i (i = B, SC) are the input voltage, output voltage, inductor current and output current of the battery/SC converter, respectively. u_i (i = B, SC) is the switch duty ratio, which serves as the control signal of battery/SC converter.

Considering the characteristics of the battery and SC as well as to extend battery lifecycle, it is desired that the battery supplies the smooth power at steady state, while SC compensates fast fluctuations. To achieve this kind of dynamic power sharing, most existing works are centralized control to generate current references for local controllers and linear PI controller is employed for local control to track the current references. To enhance reliability, scalability and economy, decentralized coordination of HESS is preferred. Moreover, the linear controllers cannot ensure system stability with fast dynamics under large operating point variation considering the high penetration of CPLs. A nonliner controller is desired to stabilize the system with large variation of CPLs with fast dynamics. To extend the life cycle of ESSs, it is also expected that the transient dynamics should be smooth. Taking into consideration all above requirements, a MPC based dynamic current sharing scheme is proposed for HESS to achieve decentralized current sharing, fast dynamics, large signal stability and optimized transient performance.

III. Proposed Controller for Single ESS System

In this section, a single ESS system with CPLs is studied and a composite MPC controller is proposed to achieve fast and smooth transient, accurate voltage regulation and large signal stability. It consists of a baseline MPC control law to track the optimal voltage and a higher-order sliding mode disturbance observer (HOSMO) for disturbances rejection.

A. Coordinate Transformation

To simplify the controller design, the dynamic model of the system in (2) is transformed to (3) with the feedback linearization technique [27],

$$\begin{cases} \dot{x}_{1i} = x_{2i} + d_{1i} \\ \dot{x}_{2i} = v_i + d_{2i} \end{cases} \tag{3}$$

where d_{1i}, d_{2i} are uncertain items, x_{1i}, x_{2i} are state variables, and v_i is the intermediate control law for the single ESS system (i = B or SC), which are given by

$$x_{1i} = \frac{1}{2}L_i i_{Li}^2 + \frac{1}{2}C_i v_{Ci}^2 \tag{4}$$

$$x_{2i} = E_i i_{Li} - \frac{v_{Ci}^2}{R_0} \tag{5}$$

$$v_i = \frac{E_i^2}{L_i} + \frac{2v_{Ci}^2}{R_{0i}^2 C_i} - \left(\frac{E_i v_{Ci}}{L_i} + \frac{2i_{Li}v_{Ci}}{R_{0i}C_i}\right)(1-u_i) \tag{6}$$

$$d_{1i} = -P_{CPLi} + \frac{v_{Ci}^2}{R_{0i}} - \frac{v_{Ci}^2}{R_i} \tag{7}$$

$$d_{2i} = \frac{2}{R_{0i}C_i}\left(P_{CPLi} - \frac{v_{Ci}^2}{R_{0i}} + \frac{v_{Ci}^2}{R_i}\right) \tag{8}$$

where R_i, R_{0i}, and P_{CPLi} (i = B or SC) represent the real-time resistive load, nominal resistive load and real-time CPL of the ESS converter system, respectively.

Then the voltage tracking objective of v_{Ci} to its reference V_{Ci} in the system (2) is converted to designing v_i for the asymptotic tracking of state x_{1i} to the reference value x_{1i}^* in the system (3), which is given by

$$x_{1i}^* = \frac{1}{2}L_i I_{Li}^2 + \frac{1}{2}C_i V_{Ci}^2 = \frac{1}{2}L_i\left(\frac{P_i}{E_i}\right)^2 + \frac{1}{2}C_i V_{Ci}^2 \tag{9}$$

where P_i is the power output of the ith ESS, given

$$P_i = P_{CPLi} + \frac{V_{Ci}^2}{R_i} = -d_{1i} + \frac{V_{Ci}^2}{R_{0i}}. \tag{10}$$

If the obtained intermediate control law v_i is designed, the final duty radio u_i in the original system (2) is calculated as

$$u_i = 1 - \left(\frac{E_i^2}{L_i} + \frac{2v_{Ci}^2}{R_{0i}^2 C_i} - v_i\right)\Big/\left(\frac{E_i v_{Ci}}{L_i} + \frac{2i_{Li}v_{Ci}}{R_{0i}C_i}\right). \tag{11}$$

B. Baseline MPC Control Law Design

Note: As the design of MPC control introduces derivatives, estimates and predictions of variables, the functions of some symbols are declared here to facilitate the explanation: the r-th order derivatives of variables are denoted by $(\bullet)^{(\mathrm{r})}$, the estimates of the variables are denoted by the hatted symbol $(\hat{\bullet})$, and the predictions of the variables within a receding horizon time interval are denoted by the barred symbol $(\bar{\bullet})$.

In this part, a baseline model predictive controller is designed first for the nominal system of (3):

$$\dot{x}_{1i} = x_{2i}, \dot{x}_{2i} = v_i. \tag{12}$$

Considering (9) and (10), we have $x_{1is} = x_{1i}^*$, $x_{2is} = \dot{x}_{1is} = -(-d_{1i} + \frac{v_{Ci}^2}{R_{0i}})\dot{d}_{1i}L_i/E_i^2$ and $v_{is} = \dot{x}_{2is} = -[(-d_{1i} + \frac{v_{Ci}^2}{R_{0i}})\ddot{d}_{1i} + \dot{d}_{1i}^2]L_i/E_i^2$.

Then the future output $\hat{y}_i(t+\tau)$ in the predictive period $(0 \le \tau \le T)$ is written by Taylor series expansion as

$$\begin{aligned}\hat{y}_i(t+\tau) &= \hat{y}_i(t) + \tau \hat{y}_i^{(1)}(t) + \cdots + \frac{\tau^{n+r}}{(n+r)!}\hat{y}_i^{(n+r)}(t) \\ &\approx x_{1i} + \tau x_{2i} + \frac{\tau^2}{2!}v_i + \frac{\tau^3}{3!}v_i^{(1)} \\ &= \begin{bmatrix} \bar{\Gamma} & \tilde{\Gamma} \end{bmatrix}\begin{bmatrix} \bar{X}_i \\ \tilde{V}_i \end{bmatrix}\end{aligned} \tag{13}$$

where $\bar{\Gamma} = [\,1 \quad \tau\,]$, $\tilde{\Gamma} = [\,\frac{\tau^2}{2!} \quad \frac{\tau^3}{3!}\,]$, $\bar{X}_i = [\,x_{1i} \quad x_{2i}\,]^\top$, $\tilde{V}_i = [\,v_i \quad v_i^{(1)}\,]^\top$ and r is the control order, which is explained in [28] in detail and it is selected to be 1 here. The symbol $v_i^{(1)}$ represents the derivative of v_i.

Based on (13), the cost function of system (12) is defined as follows

$$\begin{aligned}J_i(t) &\triangleq \frac{1}{2}\int_0^T \left[\hat{y}_i(t+\tau) - \hat{y}_{is}(t+\tau)\right]^\top \\ &\quad\times \left[\hat{y}_i(t+\tau) - \hat{y}_{is}(t+\tau)\right]d\tau \\ &= \frac{1}{2}\begin{bmatrix} \left(\bar{X}_i - \bar{X}_{is}\right)^\top & \left(\tilde{V}_i - \tilde{V}_{is}\right)^\top \end{bmatrix}\begin{bmatrix} \Gamma_1 & \Gamma_2 \\ \Gamma_2^T & \Gamma_3 \end{bmatrix}\begin{bmatrix} \bar{X}_i - \bar{X}_{is} \\ \tilde{V}_i - \tilde{V}_{is} \end{bmatrix}\end{aligned} \tag{14}$$

where $\Gamma_1 = \int_0^T \bar{\Gamma}^T\bar{\Gamma}d\tau$, $\Gamma_2 = \int_0^T \bar{\Gamma}^T\tilde{\Gamma}d\tau$, $\Gamma_3 = \int_0^T \tilde{\Gamma}^T\tilde{\Gamma}d\tau$ and $\bar{X}_{is} = [\,x_{1is} \quad x_{2is}\,]^\top$, $\tilde{} V = [\,v_{is} \quad v_{2is}\,]^\top$.

Define $\hat{V} = [v_i(t)^\top, v_i^{(1)}(t)^\top]$, the following equation holds:

$$\begin{aligned}\frac{\partial J_i}{\partial \hat{V}_i} &= \left(\frac{\partial\left(\tilde{V}_i - \tilde{V}_{is}\right)}{\partial \hat{V}_i}\right)^\top \left[\Gamma_2^\top\left(\bar{X}_i - \bar{X}_{is}\right) + \Gamma_3\left(\tilde{V}_i - \tilde{V}_{is}\right)\right] \\ &= 0.\end{aligned} \tag{15}$$

Since $\partial(\tilde{V}_i - \tilde{V}_{is})/\partial\hat{V}$ is non-singular, the optimal solution can be obtained by solving (15) as

$$\tilde{V}_i = \tilde{V}_{is} - \Gamma_3^{-1}\Gamma_2^\top\left(\bar{X}_i - \bar{X}_{is}\right). \tag{16}$$

Then the baseline MPC law can be achieved as

$$v_{mpci} = \mathcal{I}\left[\tilde{V}_{is} - \mathcal{T}_3^{-1}\mathcal{T}_2^\top\left(\bar{X}_i - \bar{X}_{is}\right)\right] = v_s - K\left(\bar{X}_i - \bar{X}_{is}\right) \tag{17}$$

where $\mathcal{I} \triangleq [\,1, \quad 0\,] \in R^{1\times 2}, K = [k_{0i}, k_{1i}]$ are the control gains to be solved.

C. HOSMO Design

After the baseline MPC law (17) is achieved, HOSMO technique is applied to estimate the uncertainties/disturbances of the system (3) (i.e., d_{1i} and d_{2i}), as this technique can estimate disturbances and their derivatives in a fast convergence rate [29], [30].

Assumption: The disturbances $d_j(t) \in L_\infty$ and $\dot{d}_j(t) \in L_\infty$ are bounded by $\sup_{t\ge 0}\|d_j(t)\| \le \bar{D}_j, \sup_{t\ge 0}\|\dot{d}_j(t)\| \le \tilde{D}_j$, for $j = 1i, 2i$, where $\bar{D}_j$ and $\tilde{D}_j$ are known positive constants.

The Assumption is satisfied for the system under study as the output power of converters and its derivative are bounded in practice.

Then observers for d_{1i} and d_{2i} are designed based on HOSMO technique as

$$\begin{cases} \dot{z}_{10i} = v_{10i} + x_{2i}, \dot{z}_{11i} = v_{11i}, \dot{z}_{12i} = v_{12i}, \dot{z}_{13i} = v_{13i} \\ v_{10i} = -3L_{1i}^{1/4}\mathrm{sig}^{3/4}(z_{10i} - x_{1i}) + z_{11i} \\ v_{11i} = -2L_{1i}^{1/3}\mathrm{sig}^{2/3}(z_{11i} - v_{10i}) + z_{12i} \\ v_{12i} = -1.5L_{1i}^{1/2}\mathrm{sig}^{1/2}(z_{12i} - v_{11i}) + z_{13i} \\ v_{13i} = -1.1L_{1i}\mathrm{sign}(z_{13i} - v_{12i}) \\ \hat{d}_{1i} = z_{11i}, \widehat{\dot{d}_{1i}} = z_{12i}, \widehat{\ddot{d}_{1i}} = z_{13i} \end{cases} \tag{18}$$

$$\begin{cases} \dot{z}_{20i} = v_{20i} + v_i, \dot{z}_{21i} = v_{21}, \dot{z}_{22i} = v_{22i} \\ v_{20i} = -2L_{2i}^{1/3}\mathrm{sig}(z_{20i} - x_{2i}) + z_{21i} \\ v_{21i} = -1.5L_{2i}^{1/2}\mathrm{sig}(z_{21i} - v_{20i}) + z_{22i} \\ v_{22i} = -1.1L_{2i}\mathrm{sign}(z_{22i} - v_{21i}) \\ \hat{d}_{2i} = z_{21i}, \widehat{\dot{d}_{2i}} = z_{22i} \end{cases} \tag{19}$$

where L_j $(i = 1, 2)$ are gains of the observers selected as $L_j > \bar{D}_j$ [29]. Function $\mathrm{sig}^a(\cdot)$ is defined by $\mathrm{sig}^a(\cdot) = \mathrm{sign}(\cdot)|\cdot|^a$, where $\mathrm{sign}(\cdot)$ denotes the sign function and $a > 0$ is a constant.

The error dynamics of (18) are derived as

$$\begin{cases} \dot{e}_{0i} = -3L_{1i}^{1/4}\mathrm{sig}^{3/4}(e_{0i}) + e_{1i} \\ \dot{e}_{1i} = -2L_{1i}^{1/3}\mathrm{sig}^{2/3}(e_{1i} - \dot{e}_{0i}) + e_{2i} \\ \dot{e}_{2i} = -1.5L_{1i}^{1/2}\mathrm{sig}^{1/2}(e_{2i} - \dot{e}_{1i}) + e_{3i} \\ \dot{e}_{3i} \in -1.1L_{1i}\mathrm{sign}(e_3 - \dot{e}_{2i}) + \left[-\bar{D}_{1i}, \bar{D}_{1i}\right] \end{cases} \tag{20}$$

where the estimation errors are defined as $e_{0i} = \hat{x}_{1i} - x_{1i}$, $e_{1i} = \hat{d}_{1i} - d_{1i}$, $e_{2i} = \widehat{\dot{d}_{1i}} - \dot{d}_{1i}$, $e_{3i} = \widehat{\ddot{d}_{1i}} - \ddot{d}_{1i}$.

According to the result in [29], the errors in (20) are finite-time stable; it is similar for the error system of d_{2i} in (19). Thus the estimated terms $\hat{d}_{1i}$, $\widehat{\dot{d}_{1i}}$, $\widehat{\ddot{d}_{1i}}$ and $\widehat{\dot{d}_{2i}}$ converge to d_{1i}, $\dot{d}_{1i}$, $\ddot{d}_{2i}$ and $\dot{d}_{2i}$ within a finite time, respectively.

D. Composite MPC Design

Inspired by the separation principle of disturbance observer based control [31] and with (17)-(19), a composite MPC law is constructed

$$\begin{aligned}v_i &= v_{mpci} - \begin{bmatrix} k_{1i} & 1 \end{bmatrix}\hat{d}_i \\ &= v_{is} - K_i\left(\bar{X}_i - \bar{X}_{is}\right) - \begin{bmatrix} k_{1i} & 1 \end{bmatrix}\hat{d}_i \\ &= v_{is} - k_{0i}(x_{1i} - x_{1is}) - k_{1i}\left(x_{2s} - x_{2s} + \hat{d}_{1i}\right) - \hat{d}_{2i}\end{aligned} \tag{21}$$

where v_{mpci} represents the baseline nonlinear MPC law (17) from (17), $\hat{d}_i$ represents the estimate of the uncertainties from (18) and (19).

Remark 1: The developed MPC controller is flexible to be applied in other types of DC/DC converters, like buck, buck-boost converters. The procedure is similar as described above. First, feedback linearization technique is applied to transform the converter model into the standard form in (3). For different types of converters, this transformation is different. For buck converter, the transformation is designed as $x_{1i} = \frac{1}{2}C_i v_{Ci}^2$. For buck-boost converter, the transformation is designed as $x_{1i} = \frac{1}{2}L_i i_{Li}^2 + \frac{1}{2}C_i v_{Ci}^2 + C_i E_i v_{Ci}$. With coordinate transformation, different converter models can be transformed into the standard form in (3). The following design steps are the same as the procedure described in Section III.B-D: a receding horizon optimization problem is formulated for optimal voltage tracking, as illustrated in (17); a higher-order sliding mode observer (HOSMO) is designed and integrated into the optimization problem to deal with the unknown load variation and system uncertainties, as presented in (18) and (19); then an explicit closed-loop solution is obtained by solving the receding horizon optimization problem offline, as shown in (21).

IV. MPC Based Dynamic Power Sharing Scheme for Hybrid Energy Storage System

In this section, a decentralized dynamic power sharing scheme is developed for the HESS based on the proposed MPC controller.

To achieve decentralized dynamic power sharing between battery and SC, a virtual resistance droop controller and a virtual capacitance droop controller are implemented for battery converter and SC converter, respectively [12]. The output voltage references for battery/SC converter are given by

$$\begin{cases} V_{CB} = V_{Cref} - R_v i_{oB} \\ V_{CSC} = V_{Cref} - \frac{1}{sC_v} i_{oSC} \end{cases} \tag{22}$$

where V_{Cref} is the voltage reference of DC bus; V_{CB} and V_{CSC} are the output voltage references for the battery and SC converter controllers, respectively. The virtual resistance R_v is determined by the maximum bus voltage variation and converter current rating. C_v is the virtual capacitance to be designed given the expected dynamics.

The output power and current of the ith source converter ($i = B, SC$) can be estimated by the HOSMO based on (1), (10) and (18), as

$$\hat{P}_i = -\hat{d}_{1i} + \frac{V_{Ci}^2}{R_{0i}} \tag{23}$$

$$\hat{i}_{oi} = \frac{-\hat{d}_{1i}}{V_{Ci}} + \frac{V_{Ci}}{R_{0i}}. \tag{24}$$

By substituting (22), (23) and (24) into (9), the reference values for battery and SC converters x_{1B}^* and x_{1SC}^* are obtained as

$$x_{1B}^* = \frac{1}{2} L_B \left(\frac{\hat{P}_B}{E_B}\right)^2 + \frac{1}{2} C_B \left(V_{Cref} - R_v \hat{i}_{oB}\right)^2 \tag{25}$$

$$x_{1SC}^* = \frac{1}{2} L_{SC} \left(\frac{\hat{P}_{SC}}{E_{SC}}\right)^2 + \frac{1}{2} C_{SC} \left(V_{Cref} - \frac{1}{C_v s} \hat{i}_{oSC}\right)^2. \tag{26}$$

With the composite MPC controller, the output voltages of the battery and SC converter systems are able to track their reference values with optimized performance. Considering the droop control for which line impedance can be neglected, we have $V_{CB} = V_{CSC} = V_{dc}$ [12]. Based on (22), the current sharing relationship between the battery and SC is obtained as follows:

$$\begin{cases} i_{oB} = G_B(s) i_o = \frac{1}{R_v C_v s + 1} i_o \\ i_{oSC} = G_{SC}(s) i_o = \frac{R_v C_v s}{R_v C_v s + 1} i_o \end{cases} \tag{27}$$

where G_B and G_{SC} can be seen as a low-pass filter and a high-pass filter with the cutoff frequency ω_c given in (28). Thus,

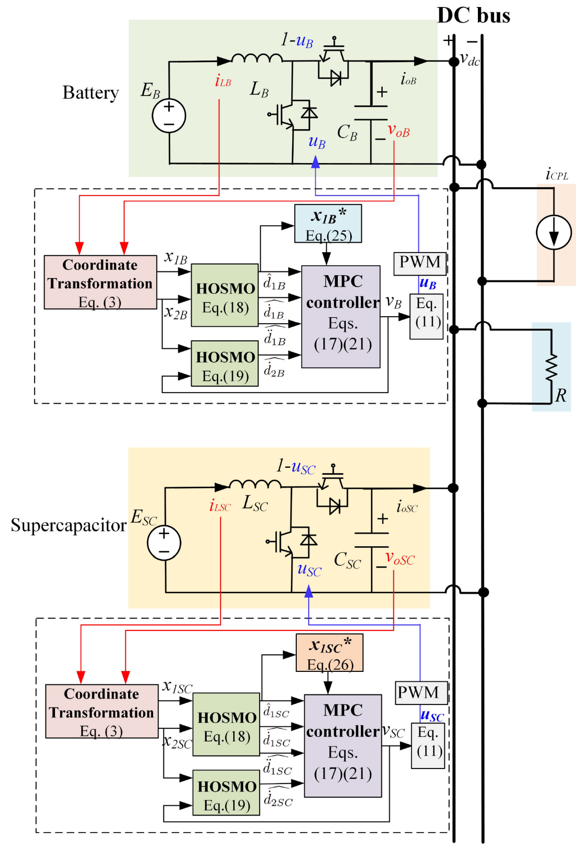

Fig. 3. The control scheme of the proposed MPC based dynamic power sharing strategy of the HESS.

the load current is automatically decoupled into low frequency part for battery and high frequency part for SC.

$$\omega_c = \frac{1}{R_v C_v}. \tag{28}$$

The coordination scheme is developed in Fig. 3 with the proposed MPC + virtual resistance droop controller and MPC + virtual capacitance droop controller for battery and SC, respectively. As can be observed, there is no communication between SC and battery, thus the decentralized dynamic power sharing is achieved. Given the expected sharing dynamics (i.e., cutoff frequency ω_c), the virtual capacitance coefficient C_v can be designed based on (28).

Remark 2: The proposed coordination scheme is flexible to be extended to hybrid energy storage systems with multiple batteries and multiple SCs. For system with m batteries and n SCs, the control of individual converter will be the same as (25) for batteries, and (26) for supercapacitors, as shown in Fig. 3. And the corresponding virtual resistance and virtual capacitance can be designed based on the expected current sharing relationship of batteries and SCs, as

$$i_{oB1} : i_{oB2} : \cdots : i_{oBm} = R_{v1}^{-1} : R_{v2}^{-1} : \cdots : R_{vm}^{-1} \tag{29}$$

$$i_{oSC1} : i_{oSC2} : \cdots : i_{oSCn} = C_{v1} : C_{v2} : \cdots : C_{vn}. \tag{30}$$

The equivalent virtual resistance of all m batteries, and equivalent virtual capacitance of all n SCs are calculated as

TABLE I
SYSTEM PARAMETERS OF TESTED SYSTEM

Variables	Description	Value
V_{Cref}	Load bus voltage reference	100 V
T	Prediction period	0.001 s
f_s	Switching frequency	20 kHz
E_{0i}	Nominal input voltage	50 V
L_{0i}	Nominal inductance	1 mH
C_{0i}	Nominal capacitance	1 mF
L_{0i}, L_{0i}	HOSMO gains	10^6, 10^8
R_v	Virtual resistance	0.5
C_v	Virtual capacitance	$1/0.5/(2*\pi*0.5)$

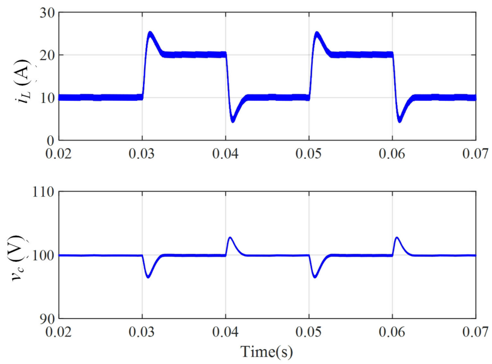

Fig. 4. Simulation results with variable CPL and resistive load for single source case.

$$R_{veq} = \left(\sum_{i=1}^{m} R_{vi}^{-1}\right)^{-1} \tag{31}$$

$$C_{veq} = \sum_{i=1}^{n} C_{vi}. \tag{32}$$

The system dynamics can be designed based on cut-off frequency to be calculated as

$$\omega_c = \frac{1}{R_{veq}C_{veq}}. \tag{33}$$

V. SIMULATION RESULTS

To verify the effectiveness in terms of stability, fast dynamics, smooth transient and accurate tracking against large disturbances of proposed method, a DC microgrid system with the proposed control strategy shown in Fig. 3 is built in MATLAB/Simulink. The detailed parameters of the system are listed in Table I.

A. Single Source Case

Only the SC is connected to the system with its interface converter to verify the effectiveness of the composite MPC controller for the optimized transient performance, accurate tracking and stabilization in a single source system with CPLs.

The simulation result of the variable CPL and resistive load for single source case is shown in Fig. 4. At the beginning, 500 W CPL is connected to the bus, while no resistive load connected. At 0.03 s and 0.04 s, 500W resistive load is connected and disconnected, respectively. At 0.05 s, the CPL increases to 1000 W. At 0.06 s, the CPL decreases back to

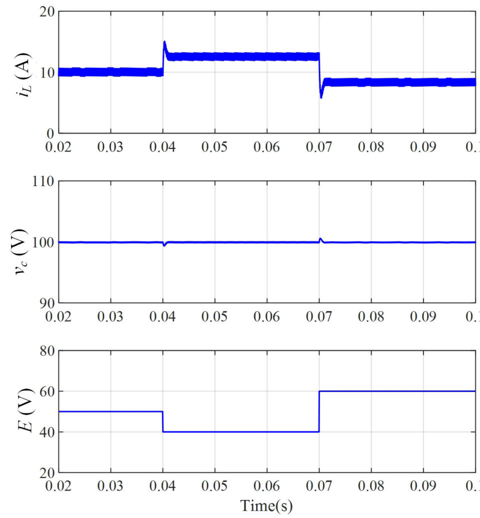

Fig. 5. Simulation results with variable source voltage for single source case (50 V-40 V-60 V).

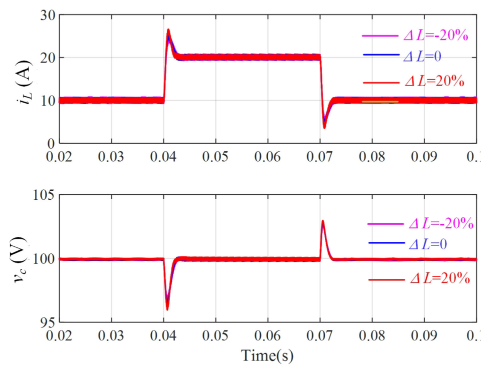

Fig. 6. Simulation results with the uncertain inductance (500 W-1000 W-500 W).

500 W. As the simulation result shows, the settling time of the transients is around 2 ms, which shows the proposed method can guarantee the smooth transient performance of the system. Moreover, the load bus voltage is regulated accurately at the reference value after the settling time. The simulation result reveals that the proposed method can achieve smooth transients with accurate tracking with the integration for both resistive load and CPL.

As reported in [22], the worst operation scenario in terms of stability is the pure CPL case, The following case studies make only CPL connected to the load bus.

Fig. 5 shows the result with variable source voltage when the load maintains at 500 W. At 0.04 s and 0.07 s, the source bus voltage E varies from 50 V to 40 V and from 40 V to 60 V, respectively. As the result shows, with the step variations of source voltage, the bus voltage is regulated accurately at 100 V in optimized dynamics within 2 ms. Thus, the system is in stable operation under the variation of input voltage.

To validate the robustness of the proposed method against model uncertainties, the simulations with uncertain inductance values and capacitance values are executed. Fig. 6 shows the system dynamic performance with different inductance

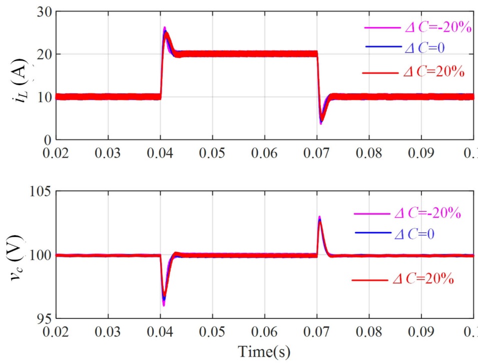

Fig. 7. Simulation results with the uncertain capacitance (500 W-1000 W-500 W).

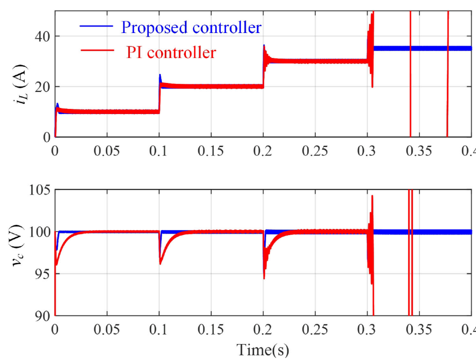

Fig. 8. Comparison results between the proposed controller and double-loop PI controller with the variation of CPL.

$L = L_0(1+\Delta L)$, where ΔL is the different deviation of inductance at -20%, 0 and 20%. As shown in Fig. 6, the system bus voltage can accurately tracks the reference value within 2 ms, and small transient deviation with step variations of load at 0.04 s and 0.07 s for each case. Thus proposed method have the good robustness against the uncertainties in inductance value for system operation. Similarly, the system dynamics with different deviation of capacitance ΔC at -20%, 0 and 20% are shown in Fig. 7. The actual capacitance C is $C_0(1 + \Delta C)$. The simulation results illustrate that proposed method can keep the output voltage accurately track the reference with different deviation capacitance. As a conclusion, the proposed method can achieve offset-free tracking with robustness against the uncertainties of the model.

To show the advantage of the proposed method in large signal stability with large CPL variation, a comparison is made against the conventional double-loop PI controller, which is illustrated in Fig. 8. The double-loop PI controller is designed based on [12] with the bandwidths for voltage and current control loops selected as 200 Hz and 2000 Hz respectively. As shown in Fig. 8, when CPL increases from 1500 W to 1750 W at 0.3 s, the PI controlled system goes to unstable while the system with proposed control method remains stable. For PI controller, there is a tradeoff between stability margin and dynamic performance. While the proposed method can achieve both faster dynamics and larger stability margin at the same time. Therefore, the advantage of the proposed controller is validated.

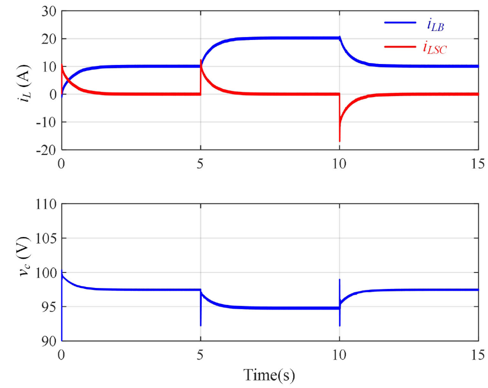

Fig. 9. Simulation results for the HESS with proposed method ($\omega_c = 0.5 * 2\pi$ rad/s).

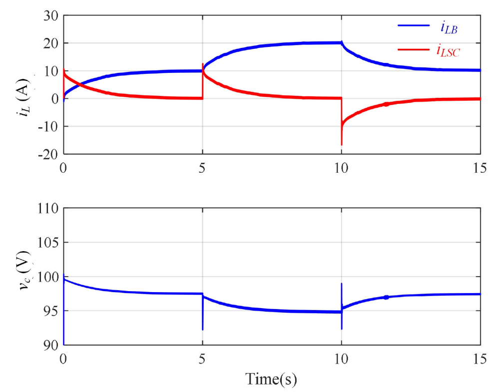

Fig. 10. Simulation results for the HESS with proposed method ($\omega_c = 0.2 * 2\pi$ rad/s).

B. Coordinated Control of HESS

To verify the proposed coordination scheme for decentralized dynamic power sharing, both the battery and SC are connected to the bus through the interface converters.

Fig. 9 shows the voltage response and current response of the battery and SC when CPL increases from 500 W to 1 kW at 5 s and decreases from 1 kW to 500 W at 10 s. As the Fig. 9 shows, when the load varies, the SC current changes immediately while the battery current changes smoothly; when at steady state, the SC provide no current while battery supplies the total power demand. Therefore, the proposed method can achieve the decentralized dynamic power sharing for the battery and SC.

To verify the effectiveness of the proposed coordination scheme to achieve different dynamic sharing requirements, simulation results with a different cutoff frequency is conducted in Fig. 10 ($\omega_c = 0.2 * 2\pi$ rad/s) with the same load profile in Fig. 9 ($\omega_c = 0.5 * 2\pi$ rad/s). It reveals that decentralized dynamic sharing is also achieved in Fig. 10 and the settling time is 2.5 times in Fig. 10 compared with that in Fig. 9, which is consistent with their cut-off frequency relationship.

To verify the effectiveness of the proposed scheme in charging mode to compensate negative equivalent load power (renewable generation is larger than load demand), simulation study under this case is conducted. Fig. 11 shows the

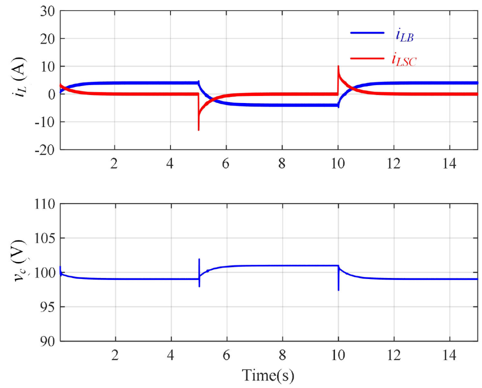

Fig. 11. Simulation results for the HESS with proposed method under charging mode ($\omega_c = 0.5 * 2\pi$ rad/s).

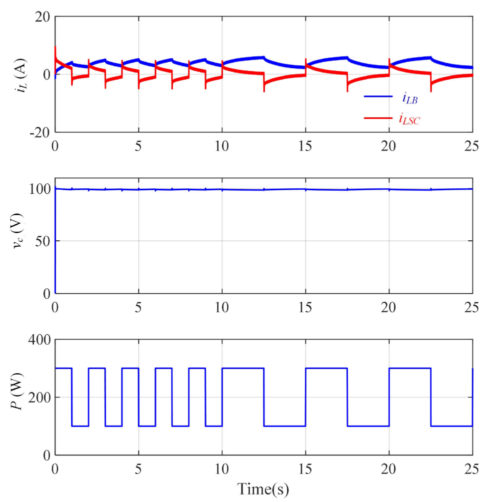

Fig. 12. Simulation results for the HESS under PPLs ($\omega_c = 0.5 * 2\pi$ rad/s).

simulation result when HESS absorbs extra power generation. Initially the equivalent load of HESS is 200 W, at 5 s, the load power reduces to be −200 W. We can see SC current increases in the negative direction immediately and decreases to zero gradually, meanwhile, battery current reduces gradually to a negative value to absorb all the extra power generation at steady state. The dynamic response is similar as the positive equivalent load case in Fig. 9. This verify the effectiveness of the proposed strategy under charging mode.

To verify the effectiveness of the proposed method to accommodate pulsed power loads (PPLs), simulation study with PPLs is conducted. Fig. 12 shows the result with the parameter in Table I ($\omega_c = 0.5*2\pi$ rad/s). The pulse frequency is set at 0.5 Hz for 0-10 s. and 0.2 Hz for 10-25 s with each cycle the load power stepping up from 100 W to 300 W, and stepping down from 300 W to 100 W. As can be observed, with each step change, SC responds immediately and battery responds smoothly. This verify the effectiveness of the proposed strategy to accommodate PPLs.

To verify the scalability of the proposed method, simulation of a system with 3 batteries and 2 SCs are conducted. Virtual resistance values R_v of Battery 1, Battery 2, Battery 3 are set at 2, 2 and 1, and the virtual capacitance values C_v of SC 1 and SC 2 are set at $1/R_{veq}/\omega_c/3$ and $1/R_{veq}/\omega_c/3 * 2$. Fig. 13 shows the simulation result. Output current of Battery 1 equals to Battery 2, and is a half of Battery 3, which verifies the relationship in (29). Similarly, output current of SC 1 during transient is a half of SC 2, which verifies the relationship in (30). Moreover, the dynamic response of system under load change is the same as Fig. 9, as the product of the designed equivalent virtual resistance of three batteries R_{veq} and the designed equivalent virtual capacitance of two SCs C_{veq} equals to the product of R_v and C_v for single HESS system given in Table I, which verifies that the dynamic response is determined by the designed cut-off frequency, as illustrated in (28) and (33).

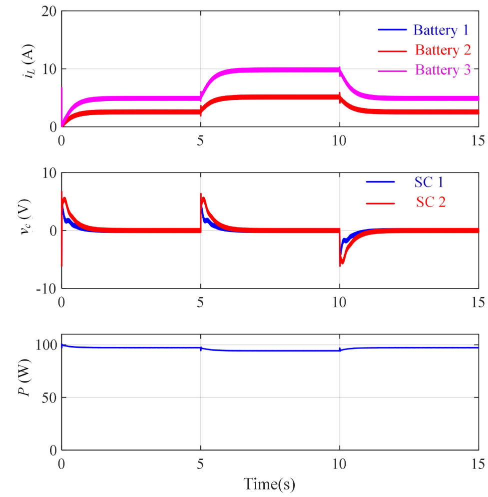

Fig. 13. Simulation results for the HESS with 3 batteries and 2 SCs ($\omega_c = 0.5 * 2\pi$ rad/s).

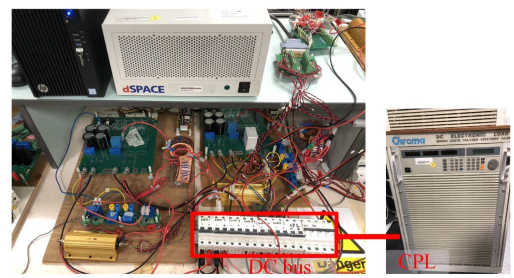

Fig. 14. Experimental setup.

VI. Experimental Results

To further validate the effectiveness of the proposed method in actual experiments, a platform of a hybrid energy storage system feeding CPL is constructed as shown in Fig. 14. The bidirectional DC/DC converters controlled by dSPACE 1006, are used to connected battery and SC to the common bus. The system parameters are the same as simulations parameters listed in Table I. Only the CPL is integrated into the system, as the worst case in terms of stability is the pure CPL.

The experimental result of the single source system with the variable CPL is presented in Fig. 15. The CPL increases from 500 W to 1 kW at t_1 and decreases from 1 kW to 500 W

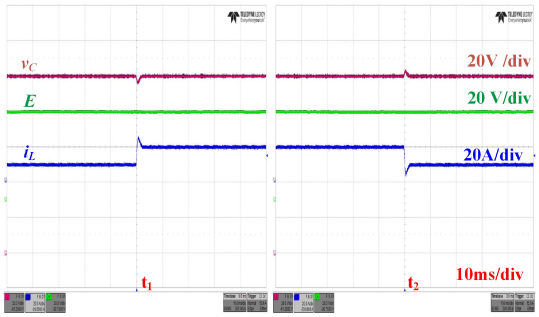

Fig. 15. Experimental results for the single source case with the CPL variation (500W-1kW-500W).

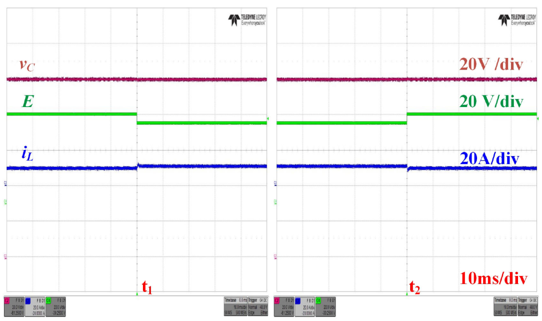

Fig. 16. Experimental results for the single source case with the input voltage variation (45V-50V-45V).

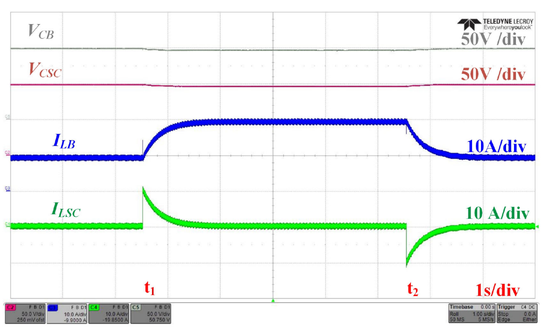

Fig. 17. Experimental results for the HESS with the proposed control method ($\omega_c = 0.5 * 2\pi$ rad/s).

at t_2. As shown in Fig. 15, with the load variation, bus voltage can accurately track the reference with smooth transient performance and the settling time is around 2ms.

Fig. 16 shows the experimental result of the single source system with the variable input voltage. The input voltage decreases from 50 V to 45 V at t_1 and increases from 45 V to 50 V at t_2. As shown in Fig. 16, with the input voltage variation, the bus voltage can be accurately regulated at 100 V with smooth transient dynamics and the settling time is around 2 ms.

Thus the proposed MPC method can ensure the stable operation with accurate tracking and smooth transients under the variation of CPLs and input voltage.

To validate the effectiveness of the coordination scheme for HESS, the experiment for the HESS with the variable CPLs is conducted. As shown in Fig. 17, the CPL increases from 500 W to 1 kW at t_1 and decreases from 1 kW to 500 W at t_2.

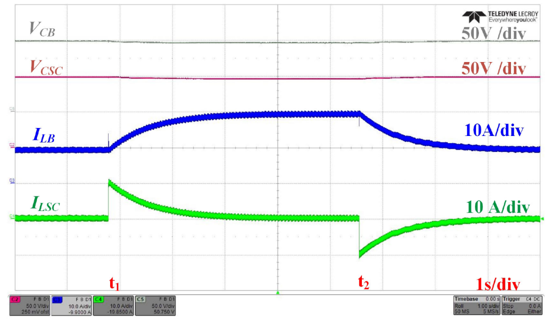

Fig. 18. Experimental results for the HESS with the proposed control method ($\omega_c = 0.2 * 2\pi$ rad/s).

The results reveal that the SC responds immediately while the battery responds smoothly with the CPL variation. Thus, the coordination scheme for HESS can achieve the decentralized dynamic power sharing.

To further validate the proposed coordination scheme in achieving expected dynamic sharing requirements, experimental result with the cutoff frequency of $\omega_c = 0.2 * 2\pi$ rad/s is conducted in Fig. 18, where the load variation is the same as in Fig. 17. The decentralized dynamic power sharing is also achieved in Fig. 18 with the transient time 2.5 times compared with that in Fig. 17. Thus, the coordination scheme ensures autonomous dynamic power sharing with the expected performance.

VII. Conclusion

This paper proposes a composite MPC based decentralized dynamic power sharing strategy for HESS feeding CPLs. First, a composite MPC is proposed for a single ESS system feeding CPL. It consists of a baseline MPC for optimal transient performance and a HOSMO to estimate uncertainties for offset free tracking. Then, a coordinated scheme is developed for HESS by using the MPC controller with the virtual resistance/capacitance droop control scheme to achieve decentralized dynamic power sharing. With the proposed scheme, the battery supplies smooth power at steady state, while the SC compensates fast fluctuations. The proposed scheme achieves a decentralized dynamic power sharing and optimized transient performance under large variation of sources and loads. Simulations and experiments are conducted to verify the proposed method. Future works will be the effective implementation of HESSs into frequency control, voltage regulation and energy management systems to stabilize power grids with high penetratio of renewables.

References

[1] D. E. Olivares *et al.*, "Trends in microgrid control," *IEEE Trans. Smart Grid*, vol. 5, no. 4, pp. 1905–1919, Jul. 2014.

[2] C. Jin, P. Wang, J. Xiao, Y. Tang, and F. H. Choo, "Implementation of hierarchical control in DC microgrids," *IEEE Trans. Ind. Electron.*, vol. 61, no. 8, pp. 4032–4042, Aug. 2014.

[3] T. Dragičević, X. Lu, J. C. Vasquez, and J. M. Guerrero, "DC microgrids—Part II: A review of power architectures, applications, and standardization issues," *IEEE Trans. Power Electron.*, vol. 31, no. 5, pp. 3528–3549, May 2016.

[4] Q. Xu, N. Vafamand, L. Chen, T. Dragičević, L. Xie, and F. Blaabjerg, "Review on advanced control technologies for bidirectional DC/DC converters in DC microgrids," *IEEE J. Emerg. Sel. Topics Power Electron.*, vol. 9, no. 2, pp. 1205–1221, Apr. 2021.

[5] J. I. Leon, E. Dominguez, L. Wu, A. M. Alcaide, M. Reyes, and J. Liu, "Hybrid energy storage systems: Concepts, advantages, and applications," *IEEE Ind. Electron. Mag.*, vol. 15, no. 1, pp. 74–88, Mar. 2021.

[6] J. Xiao, P. Wang, and L. Setyawan, "Hierarchical control of hybrid energy storage system in DC microgrids," *IEEE Trans. Ind. Electron.*, vol. 62, no. 8, pp. 4915–4924, Aug. 2015.

[7] M. M. Mardani, M. H. Khooban, A. Masoudian, and T. Dragičević, "Model predictive control of DC–DC converters to mitigate the effects of pulsed power loads in naval DC microgrids," *IEEE Trans. Ind. Electron.*, vol. 66, no. 7, pp. 5676–5685, Jul. 2019.

[8] S. Dusmez and A. Khaligh, "A supervisory power-splitting approach for a new ultracapacitor–battery vehicle deploying two propulsion machines," *IEEE Trans. Ind. Informat.*, vol. 10, no. 3, pp. 1960–1971, Aug. 2014.

[9] C. Ju, P. Wang, L. Goel, and Y. Xu, "A two-layer energy management system for microgrids with hybrid energy storage considering degradation costs," *IEEE Trans. Smart Grid*, vol. 9, no. 6, pp. 6047–6057, Nov. 2018.

[10] T. Wang, Q. Li, L. Yin, W. Chen, E. Breaz, and F. Gao, "Hierarchical power allocation method based on online extremum seeking algorithm for dual-pemfc/battery hybrid locomotive," *IEEE Trans. Veh. Technol.*, vol. 70, no. 6, pp. 5679–5692, Jun. 2021.

[11] Q. Xu, J. Xiao, X. Hu, P. Wang, and M. Y. Lee, "A decentralized power management strategy for hybrid energy storage system with autonomous bus voltage restoration and state-of-charge recovery," *IEEE Trans. Ind. Electron.*, vol. 64, no. 9, pp. 7098–7108, Sep. 2017.

[12] Q. Xu *et al.*, "A decentralized dynamic power sharing strategy for hybrid energy storage system in autonomous DC microgrid," *IEEE Trans. Ind. Electron.*, vol. 64, no. 7, pp. 5930–5941, Jul. 2017.

[13] J. Chen and Q. Song, "A decentralized dynamic load power allocation strategy for fuel cell/supercapacitor-based APU of large more electric vehicles," *IEEE Trans. Ind. Electron.*, vol. 66, no. 2, pp. 865–875, Feb. 2019.

[14] T. Dragičević, X. Lu, J. C. Vasquez, and J. M. Guerrero, "DC microgrids—Part I: A review of control strategies and stabilization techniques," *IEEE Trans. Power Electron.*, vol. 31, no. 7, pp. 4876–4891, Jul. 2016.

[15] A. Emadi, A. Khaligh, C. H. Rivetta, and G. A. Williamson, "Constant power loads and negative impedance instability in automotive systems: Definition, modeling, stability, and control of power electronic converters and motor drives," *IEEE Trans. Veh. Technol.*, vol. 55, no. 4, pp. 1112–1125, Jul. 2006.

[16] M. Cespedes, L. Xing, and J. Sun, "Constant-power load system stabilization by passive damping," *IEEE Trans. Power Electron.*, vol. 26, no. 7, pp. 1832–1836, Jul. 2011.

[17] M. Wang, Y. He, X. Xu, Z. Dong, and Y. Lei, "A review of AC and DC electric springs," *IEEE Access*, vol. 9, pp. 14398–14408, 2021.

[18] M.-H. Wang, S.-C. Tan, C.-K. Lee, and S. Y. Hui, "A configuration of storage system for DC microgrids," *IEEE Trans. Power Electron.*, vol. 33, no. 5, pp. 3722–3733, May 2018.

[19] M.-H. Wang, S. Yan, S.-C. Tan, and S. Y. Hui, "Hybrid-DC electric springs for DC voltage regulation and harmonic cancellation in DC microgrids," *IEEE Trans. Power Electron.*, vol. 33, no. 2, pp. 1167–1177, Feb. 2018.

[20] X. Lu, K. Sun, J. M. Guerrero, J. C. Vasquez, L. Huang, and J. Wang, "Stability enhancement based on virtual impedance for DC microgrids with constant power loads," *IEEE Trans. Smart Grid*, vol. 6, no. 6, pp. 2770–2783, Nov. 2015.

[21] W. Jiang, X. Zhang, F. Guo, J. Chen, P. Wang, and L. H. Koh, "Large-signal stability of interleave boost converter system with constant power load using sliding-mode control," *IEEE Trans. Ind. Electron.*, vol. 67, no. 11, pp. 9450–9459, Nov. 2020.

[22] Q. Xu, C. Zhang, C. Wen, and P. Wang, "A novel composite nonlinear controller for stabilization of constant power load in DC microgrid," *IEEE Trans. Smart Grid*, vol. 10, no. 1, pp. 752–761, Jan. 2019.

[23] Q. Xu, W. Jiang, F. Blaabjerg, C. Zhang, X. Zhang, and T. Fernando, "Backstepping control for large signal stability of high boost ratio interleaved converter interfaced DC microgrids with constant power loads," *IEEE Trans. Power Electron.*, vol. 35, no. 5, pp. 5397–5407, May 2020.

[24] M. A. Hassan, E.-P. Li, X. Li, T. Li, C. Duan, and S. Chi, "Adaptive passivity-based control of DC–DC buck power converter with constant power load in DC microgrid systems," *IEEE J. Emerg. Sel. Topics Power Electron.*, vol. 7, no. 3, pp. 2029–2040, Sep. 2019.

[25] Q. Xu, F. Blaabjerg, C. Zhang, J. Yang, S. Li, and J. Xiao, "An offset-free model predictive controller for DC/DC boost converter feeding constant power loads in DC microgrids," in *Proc. 45th Annu. Conf. IEEE Ind. Electron. Soc. (IECON)*, vol. 1. Lisbon, Portugal, 2019, pp. 4045–4049.

[26] Q. Xu, Y. Yan, C. Zhang, T. Dragicevic, and F. Blaabjerg, "An offset-free composite model predictive control strategy for DC/DC buck converter feeding constant power loads," *IEEE Trans. Power Electron.*, vol. 35, no. 5, pp. 5331–5342, May 2020.

[27] H. Sira-Ramirez and M. Ilic-Spong, "Exact linearization in switched-mode DC-to-DC power converters," *Int. J. Control*, vol. 50, no. 2, pp. 511–524, 1989.

[28] W.-H. Chen, D. J. Ballance, and P. J. Gawthrop, "Optimal control of nonlinear systems: A predictive control approach," *Automatica*, vol. 39, no. 4, pp. 633–641, 2003.

[29] A. Levant, "Higher-order sliding modes, differentiation and output-feedback control," *Int. J. Control*, vol. 76, nos. 9–10, pp. 924–941, 2003.

[30] C. Zhang, Y. Yan, A. Narayan, and H. Yu, "Practically oriented finite-time control design and implementation: Application to a series elastic actuator," *IEEE Trans. Ind. Electron.*, vol. 65, no. 5, pp. 4166–4176, May 2018.

[31] J. Yang, W. X. Zheng, S. Li, B. Wu, and M. Cheng, "Design of a prediction-accuracy-enhanced continuous-time MPC for disturbed systems via a disturbance observer," *IEEE Trans. Ind. Electron.*, vol. 62, no. 9, pp. 5807–5816, Sep. 2015.

Mengfan Zhang (Member, IEEE) received the B.S. degree and the M.S. degree in electrical engineering from the Nanjing University of Aeronautics and Astronautics, Nanjing, China, in 2015 and 2018, respectively, and the Ph.D. degree in power electronic engineering from Aalborg University, Aalborg, Denmark, in 2022. He was a Guest Ph.D. student with KTH, Sweden from November 2020 to May 2021. He is currently a Postdoctoral Researcher with the KTH Royal Institute of Technology, Sweden. His research interests include the modeling and stability analysis of the power electronic based power systems.

Qianwen Xu (Member, IEEE) received the B.Sc. degree in electrical engineering from Tianjin University, China, in 2014, and Ph.D. degree in electrical engineering from Nanyang Technological University, Singapore, in 2018. Then she worked as a Postdoctoral Research Fellow with Aalborg University, Denmark and a Wallenberg-NTU Presidential Postdoctoral Fellow with Nanyang Technological University, Singapore from 2018 to 2020. She was also a Visiting Researcher with Imperial College London from March 2020 to June 2020. Currently she is an Assistant Professor with Department of Electric Power and Energy Systems, KTH Royal Institute of Technology, Sweden. She serves as a Vice Chair with IEEE Power and Energy Society & Power Electronics Society, Sweden Chapter, and an Associate Editor for IEEE TRANSACTIONS ON SMART GRID and *IEEE Journal of Emerging and Selected Topics in Power Electronics*. She is also a recipient of Humboldt Research Fellowship, Excellent Doctorate Research Work in Nanyang Technological University, and Best paper award in IEEE PEDG 2020, etc. Her research interests include advanced control, optimization and AI application for microgrid, and smart grid.

Chuanlin Zhang (Senior Member, IEEE) received the B.S. degree in mathematics and the Ph.D. degree in control theory and control engineering from the School of Automation, Southeast University, Nanjing, China, in 2008 and 2014, respectively. Since 2014, he has been with the College of Automation Engineering, Shanghai University of Electric Power, Shanghai, where he is currently a Professor. He was a Visiting Ph.D. Student with the Department of Electrical and Computer Engineering, University of Texas at San Antonio, USA, from 2011 to 2012; a Visiting Scholar with the Energy Research Institute, Nanyang Technological University, Singapore, from 2016 to 2017; and a Visiting Scholar with Advanced Robotics Center, National University of Singapore, from 2017 to 2018. His research interests include nonlinear system control theory and applications for power systems.

Lars Nordström (Senior Member, IEEE) is Professor in information systems for power system control with KTH-The Royal Institute of Technology, Stockholm, Sweden. He is Head of the Division of Electric Power and Energy Systems with KTH and Deputy Head of the School of Electrical Engineering and Computer Science with specific responsibility for faculty development. His research and teaching is focused on issues at the crossroads of control, communication and power systems. His research interests include future architectures, functionality and quality aspects of information and communication systems used for power system control, operation, automation, and protection. He has served as Director of the Swedish Centre of Electric Power Engineering and as Thematic Leader for Smartgrids and electric storage in KIC InnoEnergy. In 2014 he was Visiting Professor with Washington State University. He is the author of 100+ scientific papers in journals and international conferences,ăa senior member of the CIRED and Cigre.

Frede Blaabjerg (Fellow, IEEE) received the Ph.D. degree in electrical engineering from Aalborg University, in 1995.

He was with ABB-Scandia, Randers, Denmark, from 1987 to 1988. He became an Assistant Professor in 1992, an Associate Professor in 1996, and a Full Professor of power electronics and drives in 1998. From 2017 he became a Villum Investigator. He is Honoris Causa with University Politehnica Timisoara (UPT), Romania and Tallinn Technical University (TTU) in Estonia. He has published more than 600 journal papers in the fields of power electronics and its applications. He is the coauthor of four monographs and editor of ten books in power electronics and its applications. His current research interests include power electronics and its applications such as in wind turbines, PV systems, reliability, harmonics, and adjustable speed drives.

He received the 31st IEEE Prize Paper Awards, the IEEE PELS Distinguished Service Award, in 2009, the EPE-PEMC Council Award, in 2010, the IEEE William E. Newell Power Electronics Award 2014, the Villum Kann Rasmussen Research Award 2014, and the Global Energy Prize, in 2019. He was the Editor-in-Chief of the IEEE TRANSACTIONS ON POWER ELECTRONICS from 2006 to 2012. He has been a Distinguished Lecturer for the IEEE Power Electronics Society from 2005 to 2007 and for the IEEE Industry Applications Society from 2010 to 2011 as well as 2017 to 2018. From 2019 to 2020 he serves a President of IEEE Power Electronics Society. He is also a Vice-President of the Danish Academy of Technical Sciences. He is nominated to be between the most 250 cited researchers in Engineering in the world by Thomson Reuters in 2014–2018.